AIP | Journal of Applied Physics

Diamond heat sinking of terahertz antennas for continuous-wave photomixing

T. Ackemann, M. Alduraibi, S. Campbell, S. Keatings, P. Luke Sam et al.

Citation: J. Appl. Phys. **112**, 123109 (2012); doi: 10.1063/1.4770460
View online: http://dx.doi.org/10.1063/1.4770460
View Table of Contents: http://jap.aip.org/resource/1/JAPIAU/v112/i12
Published by the American Institute of Physics.

Diamond heat sinking of terahertz antennas for continuous-wave photomixing

T. Ackemann,[1,a)] M. Alduraibi,[2,b)] S. Campbell,[1] S. Keatings,[1] P. Luke Sam,[1] H. Fraser,[1,c)] A. S. Arnold,[1] E. Riis,[1] and M. Missous[2]
[1]*SUPA and Department of Physics, University of Strathclyde, Glasgow G4 0NG, Scotland, United Kingdom*
[2]*School of Electrical and Electronic Engineering, The University of Manchester, Manchester, M60 1QD, United Kingdom*

(Received 4 September 2012; accepted 12 November 2012; published online 21 December 2012)

The generation of cw Terahertz radiation from photomixing in low-temperature grown GaAs is limited by the thermal load for single emitters. We propose a new heat sinking scheme based on high thermal conductivity, transparent crystalline heat spreaders as diamond in direct contact with the active zone. A first working device based on recessed electrodes is demonstrated and has a significant power dissipation capability of more than 0.75 W (average). The electrical and terahertz characteristics are analyzed. © *2012 American Institute of Physics*. [http://dx.doi.org/10.1063/1.4770460]

I. INTRODUCTION

Terahertz radiation is an upcoming technology in medical diagnosis, material inspection, quality control, short-haul wireless communications, and security applications as many materials of interest have spectral fingerprints in that region, while many packaging materials (e.g., cloth) are transparent and hence do not obstruct investigations.[1,2] In the scientific realm, terahertz radiation is important for spectroscopic investigations and characterization of modern materials and for astronomical applications, e.g., as local oscillators for Terahertz telescopes. Large scale utilization is currently limited by the lack of inexpensive, robust, compact, and sufficiently high-powered sources. Tunable cw terahertz radiation is not only imperative for narrow-band applications such as high-resolution spectroscopy and local oscillators in astronomy but also for lower resolution spectroscopy and sensing to avoid the large footprint and costs of mode-locked photo-switching systems. A convenient and attractive way to generate narrow-band cw terahertz radiation is photomixing of two infrared lasers in an antenna on low-temperature grown GaAs (LT-GaAs).[3–6] LT-GaAs is a popular material because it combines high dark resistivity, high carrier mobility, and carrier lifetimes down to 100 fs.[7] However, the maximum achievable THz-power is quite limited (to about 1 μW at 1 THz,[8–10]), which is not sufficient for many applications. Alternatively, one can use uni-traveling carrier-photodiodes (UTCPs) with a maximal power of about 10 μW at 1 THz[11] and 20 μW at 0.9 THz.[12] Quantum cascade lasers can reach powers of some tens of mW, but operate typically at a few THz and still demand cryogenic cooling.[1,13] CW THz radiation can also be generated by difference frequency generation in nonlinear crystals but due to the high intensity requirements resonant enhancement in a cavity is required.[14–16] Milliwatt power levels[15] and significant tuning[17] can be obtained. In spite of these impressive advances, fast, continuous tuning, and the efficiency realised from direct electrical pumping makes systems based on thermally tuned distributed-feedback (DFB) lasers[18–20] very attractive and LT-GaAs (or LT-InGaAs for applications in the telecommunication wavelength range) are still the dominant materials in the frequency range around 1 THz.

The power limitations in photomixing using LT-GaAs are mainly due to thermal failure of the semiconductor structure rather than the available optical input power.[6,8,9] From Ref. 8, the intensity limit is about 2 mW/μm^2 at 810 nm leading to a temperature rise of over 100 K in a 6 μm diameter pump spot. Often a damage threshold of 1 mW/μm^2 is given for 780-800 nm radiation.[9,21] One option to circumvent this is to increase the total power at constant intensity by moving to large area emitters, but their efficiency is much lower than that of small-area antenna coupled emitters.[6] With arrays of small emitters, a higher total power can be obtained,[21–23] but at present experimental investigations mostly concentrate on pulsed excitation and numerical analysis indicates a sublinear increase of total power with array size,[21] i.e., a large array does not reach the efficiency of single emitters.

For an enhancement of the power handling capability of single emitters, improved heat sinking is mandatory. In Ref. 8 some benefit of cooling the sample was demonstrated to 77 K, which was interpreted to be due to the increased thermal conductivity of GaAs at low temperatures. Buffer layers of AlAs were also tried due to its higher heat conductivity with some benefit (max. power of about 2 μW at 1 THz[9,24]) but the technology has not been taken up to widespread use. Reference 8 suggests the possibility of growing LT-GaAs on substrates of higher thermal conductivity such as diamond or Si, but so far only the variant with Si was realized and provided only a moderate increase in output power.[25] In this work, we propose and implement the use of transparent crystalline heatspreaders with a high thermal conductivity like diamond or SiC, placing them directly on top of the active layers by capillary bonding[26] *after growth is completed*. Alternatively, where optical quality is not required, the active layers can be soldered onto

[a)]Electronic mail: thorsten.ackemann@strath.ac.uk.
[b)]Present address: Department of Physics and Astronomy, College of Science, King Saud University, P.O. Box 2455, Riyadh 11451, Saudi Arabia.
[c)]Present address: Astronomy Division, Department of Physical Sciences, CEPSAR, The Open University, Walton Hall, Milton Keynes MK7 6AA, United Kingdom.

diamonds, if the structure is grown upside down and the substrate removed afterwards.[27,28] Both approaches relax the requirements on lattice matching as direct growth of semiconductor layers on crystalline dielectrics is not required (Ref. 29 suggests circumventing this limitation by growing amorphous or nano-crystalline Si on SiC or diamond, but no devices have been reported, yet). This ensures closest proximity of the headspreader to the area (within only a micrometer of the surface) where the heat is actually generated, without intermediate layers of lower thermal conductivity. Our approach stems from experience gained in heat sinking of vertical-external-cavity surface-emitting lasers (VECSELs), also referred to as semiconductor disk lasers, e.g., Refs. 27 and 30–33. These can handle tens of Watts of pump power.

II. SAMPLE PREPARATION

From a simple thermal model used also for laser modeling[28] for a thin heated disk on a semi-infinite substrate, the temperature rise ΔT can be related to the dissipated power P_{diss} by

$$\Delta T = \frac{1}{2\lambda_c D} P_{\mathrm{diss}}, \tag{1}$$

where λ_c represents the thermal conductivity, D the diameter of the heated area and the fraction represents the thermal resistance. The thermal conductivity of GaAs at room temperature is 44 W/(mK) and that of LT-GaAs only about half as large.[34] Since the latter is very thin (typically about 1 μm), it is enough to look at the GaAs and for a laser spot size of 6 μm this simple model reproduces the room temperature observations in Ref. 8 with good accuracy. The conductivity of AlAs and Si is about 2–3 times larger than that of GaAs, hence the benefit is moderate. In contrast, diamond has a thermal conductivity of about $2 \times 10^3 \mathrm{W/(mK)}$, which indicates tremendous potential for improvements. For example, detailed simulations for realistic VECSEL geometries show that in going from GaAs to diamond heat sinking the temperature rise in a 10 W, 50 μm diameter pump spot can be reduced from about 280 K to 70 K.[32] Equation (1) suggests a best-case scenario of an improvement of the photocurrent generated by the input power of $2000/44 \approx 45$. If we assume only that the incident optical power can be increased by a factor of 10 before thermal failure sets in (very well supported by the experience in VECSELs), due to the quadratic dependence of the THz output power on photocurrent or optical input power, respectively, this indicates a potential increase of the output power by a factor of 100. We stress that the benefit of developing this heat sinking technique is not limited to single emitters based on LT-GaAs, but would be also beneficial for power scaling UTCPs and possibly arrays of LT-GaAs or UTCPs.

There are two main options to position the heat sink (Ref. 33, see Fig. 1). The first is to provide an etch stop between the active layer and substrate and to transfer the active layer onto the diamond after substrate removal. In that case one can use an inexpensive CVD diamond of low optical quality but the heat sink is still a few microns away from the active layer and one needs to handle a very thin specimen

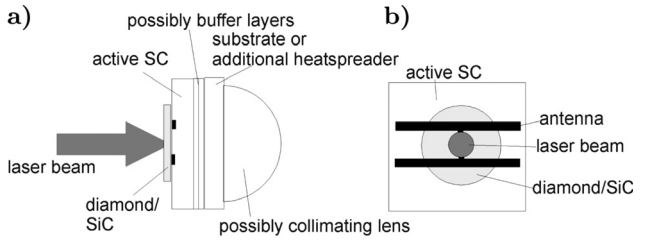

FIG. 1. Side view (a) and front view (b) of the scheme proposed and realized (black: metallization, light gray: diamond, dark gray: laser beam).

in between. Alternatively, one would need to develop a process in which the structure is grown upside-down, soldered to the diamond and then the substrate is removed from the LT-GaAs by etching.[27] The second option is to attach the diamond to the wafer surface by capillary bonding.[30,31] This is a relatively simple process but demands an optical quality diamond. In line with many VECSEL experiments, it was decided to implement the second option for demonstration purposes and use a natural, wedged diamond (0.6–0.74 mm thick, 5 mm diameter) with a broad-band anti-reflection coating on the side opposite to the wafer. This option reduces somewhat the directionality of emission because the THz radiation goes preferentially into the half-plane with the higher dielectric constant but even with the diamond on the front the situation is not symmetric (the ratio between the dielectric constants of GaAs and diamond is about 2.3) and the reduction is at most 50%, which can be easily compensated for by increased output power, if the heat sinking scheme has the benefits anticipated.

For the samples, a buffer layer of GaAs with a thickness of about 240 nm is grown on a semi-insulating GaAs substrate at 580 °C, followed by the LT-GaAs grown at 250 °C with a nominal thickness of 1 μm. In order to allow the diamond disk to be in contact with the surface of the LT-GaAs layer, recessed Ti/Au contacts were deposited. Although this provides a complication for the process, we note that there are indications that buried electrodes might provide additional benefit for efficiency because of an improvement of the electrical field distribution in the active region.[10,35] Trenches, 200 nm deep, were etched into a 1 μm-thick LT-GaAs layer with the shape of the desired contacts. Then, approximately 170 nm-thick Ti/Au contacts were deposited. Standard dipole and bow tie antenna profiles were used with gaps in the 10–20 μm range fed by common bias lines (see Fig. 2(a), the three left rows contain bow-ties, the right one dipoles, central gaps are not resolved).

Two samples were processed. Sample 1 was furnace annealed at 550 °C for 10 min, sample 2 underwent rapid thermal annealing (RTA) at 650 °C for about 10 min. The dark resistance of sample 1 was measured to be 120 MΩ. Since it contains 36 antennas in parallel, this translates to 4.3 GΩ per antenna (assuming equal partition), which is a typical value for LT-GaAs. A reference sample from the same MBE-batch and with the same annealing condition (furnace annealed at 550 °C) was also produced. It had, however, a conventional metallization with antenna pads on top of the semiconductor, which were contacted with probe tips. For these antennas, a dark resistance on the order of 1–2 GΩ

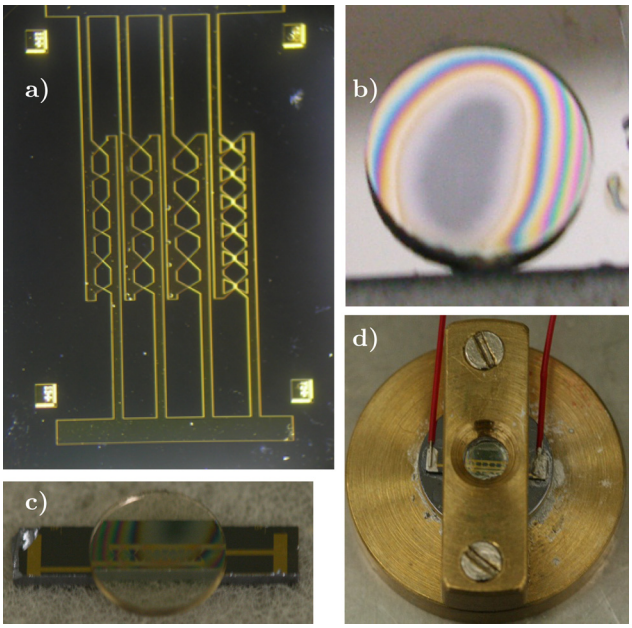

FIG. 2. (a) Image of processed sample 2 (9.5×5 mm distance between and length of outer contact pads on top and bottom), (b) LT-GaAs wafer (not processed) with partially bonded diamond (diam. 5 mm.), (c) part of sample 2 with partially bonded diamond and (d) mounted sample from (c) with wires for biasing. The homogeneous dark regions in (b) and (c) indicate good bonding, the colored interference fringes a change of gap thickness between wafer and diamond by half a wavelength.

was found. After several cycles of bonding and unbonding the diamond the dark resistance of the array dropped to 50 MΩ, indicating some contamination of the LT-GaAs. For sample 2, the dark resistance of the whole array was determined initially to be 0.5 GΩ. It also dropped during bonding attempts (see Fig. 2(c)) and was 170 MΩ (giving about 1 GΩ per antenna) in the final mounting of a single line of 6 antennas.

In these first samples only partial capillary bonding was achieved, irrespective of whether the wafer was processed (Fig. 2(c)) or not (Fig. 2(b)). This partial bonding is obvious from the presence of the interference fringes in Figs. 2(b) and 2(c). The reason for this is currently not clear though it is known that bonding becomes more difficult to achieve, if the wafer is larger than the diamond (in the present design, a part of the wafer needs to be available for contacts to supply the bias voltage). Hence the bonding was supported by mechanical strain, until homogeneous interference conditions were obtained. The mounted and bonded sample is shown in Fig. 2(d). A hemispherical Si lens (the dark disk below the wafer surrounded by the outer brass ring) is placed at the back of the wafer to reduce the divergence of the emitted THz radiation and the whole assembly is held together by mechanical pressure (via the screws through the front brass slab). Optical access for the infrared beams is provided via the central bore, which is centered on the diamond.

III. EXPERIMENTAL METHODS AND RESULTS

For sample 1, photocurrent measurements were performed with a cw TiSa laser at 800 nm, whilst for sample 2 a cw diode laser at 780 nm was used. For the THz measurements of sample 2, two cw, tunable external-cavity lasers at 780 nm are coupled to polarization-maintaining single-mode fibers, combined in a 50:50 fiber splitter and amplified in a fiber-coupled tapered amplifier. The output beam is chopped at 2 kHz and focused onto the sample with a maximal on-power of slightly less than 500 mW. A cryogenic bolometer and a lock-in amplifier are used for detection of the THz radiation. A teflon lens is used to focus the output of the antenna onto the detector in the bolometer.

Typical results for the dependence of the photocurrent on input power are shown in Fig. 3. For high enough input power (20–50 mW, depending on the antenna), the photocurrent shows a linear increase with power though the existence of an offset indicates some non-ohmic behavior. The latter is directly apparent in the low power regime. After subtraction of this offset, a log-log plot yields a scaling exponent close to 1 (with a span between 0.98 and 1.06), i.e., it confirms the expected linear scaling of photocurrent with incident power. The slope efficiency is about 0.3–0.4 μA/mW for sample 1, and 1–1.5 μA/mW for sample 2 at 20 V (the examples shown in Fig. 3 have 0.4 and 1.1 μA/mW). It depends obviously on bias voltage, reaching, e.g., 2.6 μA/mW for 32 V for the example shown in Fig. 3. This is in line with the observations in the reference sample yielding between 0.14 and 0.6 μA/mW at 20 V (depending on antenna and excitation condition) and showing also typically a non-ohmic behavior at low power, i.e., the data are in a reasonable range and the processing and mounting did not deteriorate the opto-electrical properties of the samples, but sample 2 actually indicates the potential for a higher efficiency of the recessed samples (as indicated in Refs. 10 and 35).

The modified samples are THz-active as demonstrated in Fig. 4 for three beating frequencies. The beat frequency is kept below 300 GHz because the sensitivity of the bolometer begins to drop beyond 500 GHz and hence the signal coming from the beating can be distinguished most easily from the background thermal radiation (generated by the heating due to non-radiative recombination and ohmic heating), which is

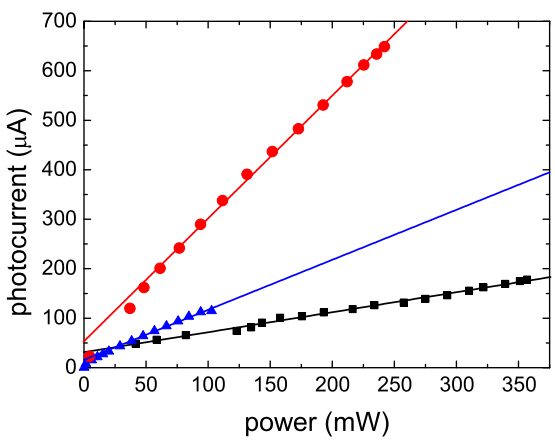

FIG. 3. Examples of photocurrent versus optical power characteristics for different antennas, with linear fits. Squares (black): sample 1, 1B (dipole, 16 μm gap), 20 V bias; triangles (blue): sample 2, 1 E (dipole, 16 μm gap), 20 V bias; circles (red): sample 2, 4 E (bow tie, 20 μm gap), 32 V bias (for 4 E, power and photocurrent refer to averaged quantities due to chopping). Input beam size about 11 μm ($1/e^2$-radius).

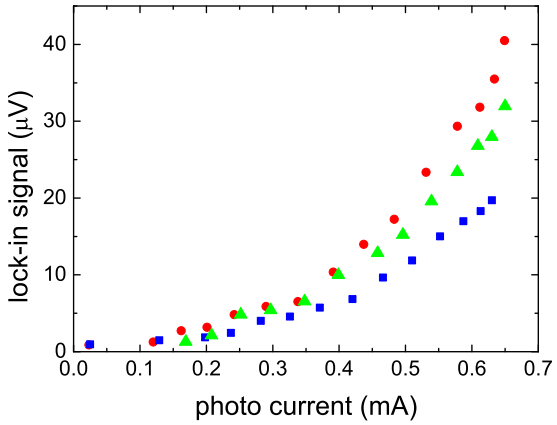

FIG. 4. Lock-in signal proportional to THz power vs. average photocurrent for sample 2, antenna 4E at 32 V (see Fig. 3 for current vs. power characteristics) at different beating frequencies: 0.25 THz (red circles), 0.32 THz (blue squares), 0.35 THz (green triangles).

also correlated with the chopping frequency. It was checked that the signal with one laser alone at the same photocurrent is only in the range of a few μV, i.e., the dominant part of the signal stems from photomixing. This is confirmed by the fact that log-log plots yield a scaling exponent of 2.05–2.28 ± 0.1, i.e., the expected quadratic scaling of THz power with photocurrent. We mention for completeness that, using an approximate calibration of the bolometer, the detected power can be estimated to be on the order of nWs. However, in these investigations no emphasis was put into achieving a high collection efficiency of the optical system coupling the radiation to the bolometer so that no conclusion on the emitted power is possible.

As a higher optical input power was not available in this work, the bias voltage was increased for further stress measurements. Fig. 5(a) shows the results for the two samples. There is a very strong non-ohmic, super-linear increase of photocurrent versus bias. Sample 1 failed at a bias of 60 V, an optical power of 456 mW and a photocurrent of 5.6 mA. This is a fairly high value, the dissipated power is 792 mW. It was found that the failure was actually in the feeding lines, not the semiconductor gap. Sample 2 failed at 90 V, an average optical power of 240 mW, and an average photocurrent of 5.72 mA. Again the dissipated power is fairly high, 755 mW (average). This time, the observation of a dark streak across the semiconductor gap indicates dielectric breakdown. From Eq. (1), one expects a temperature rise of more than 400 K for pure GaAs-based heat-sinking and about 9 K for an optimally contacted diamond. This indicates that the diamond heat sinking is working, at least to a considerable extent, and that probably the remaining limitation might be dielectric breakdown. The relationship between temporal (τ) and spatial (s) scales for diffusive processes (diffusion constant D) is roughly given by $\tau = s^2/D$. Taking the width of the gap of sample 2 as a typical (conservative) length scale, $s = 20\,\mu$m, and a thermal diffusivity of GaAs of $D = 2.5 \times 10^{-5} - 1.3 \times 10^{-4}\,\mathrm{m^2/s}$,[36,37] one obtains $\tau = 16 - 3\,\mu$s, i.e., the thermal response should be much faster than the chopping period and the peak temperature rise hence closer to 800 K, without diamond, illustrating further

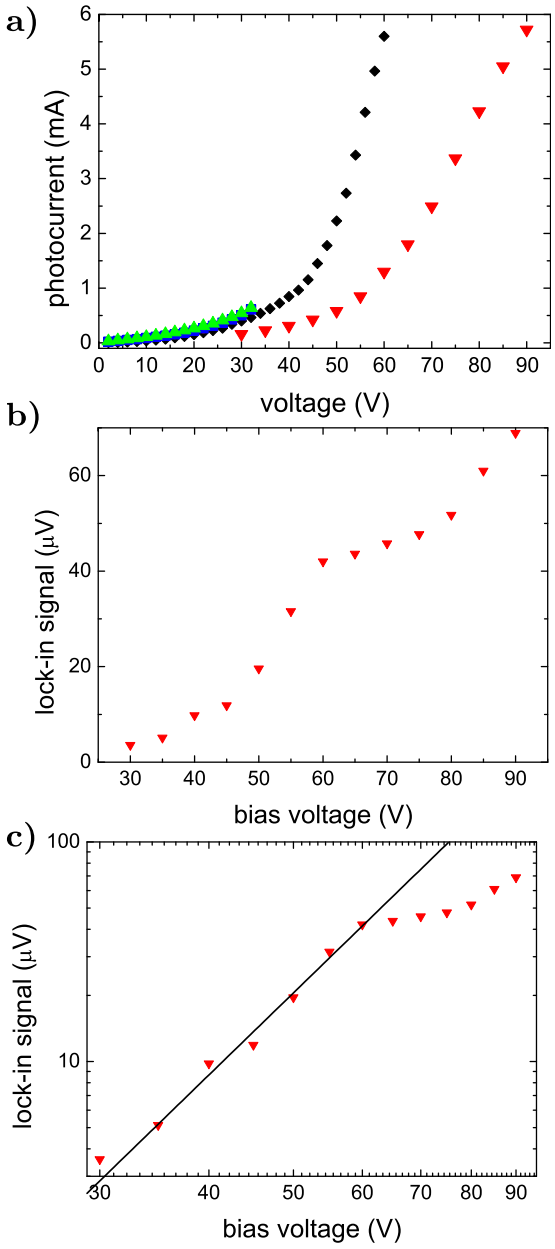

FIG. 5. (a) Photocurrent vs. bias voltage for sample 1 (black diamonds) at 456 mW optical input power and for sample 2, antenna 4E, at 240 mW average optical input power (for sample 2, the data represent an average photocurrent). Legend for sample 2 as for Fig. 4 plus high-voltage data (30–90 V) obtained one day later at 0.25 THz (red down-triangles). The low and the high voltage curves for sample 2 were obtained at two consequent days and do not match at 30 V. The reduction of photocurrent between days 1 and 2 is presumably due to a drift in alignment. Due to the failure of the sample on day 2, the data could not be retaken. A linear down-scaling of the low voltage measurements (2–32 V) to meet the value obtained at 30 V on day 2 indicates a smooth transition supporting the hypothesis of misalignment. (b) Lock-in signal proportional to THz power versus bias voltage at 0.25 THz. (c) As for (b), but in log-log plot with a linear fit to a subset of the data.

the importance of heat sinking (for the diamond scheme the thermal relaxation time should be even lower, about 0.5 μs).

Fig. 5(b) indicates, however, that the increase of photocurrent obtained at high bias voltages is not matched by a corresponding increase in THz power, but the output seems to saturate at about 60 V (beyond 1 mA photocurrent), though it picks up again somewhat beyond 80 V (beyond

4 mA). In order to investigate possible mechanisms, Fig. 5(c) shows a log-log plot of the THz-voltage characteristic. It is fairly linear for low voltages (30–60 V) with a scaling exponent of 3.9 ± 0.2. From a simple ohmic theory (e.g., Ref. 9), one expects a linear scaling of current with voltage and hence a quadratic dependence of THz power on voltage. An approximately quartic dependence of THz power on bias voltage as observed here is also reported in the literature.[10,38] In the interdigitized antennas with a finger spacing between 0.3 and 1.8 μm used in these studies, the crossover occurs between 5 and 15 V/μm. It is related to space-charge effects causing a non-ohmic, quadratic increase of photocurrent versus voltage and, via the quadratic dependence of THz power on photocurrent, a quartic increase of the THz power with voltage. In our antennas, a quadratic behavior of photocurrent versus voltage is the typical behavior already at low bias fields, including commercial samples from BATOP.[39] For example, for the curve for sample 1 displayed in Fig. 5(a) one obtains a scaling exponent of current versus voltage of 2.0 ± 0.1 for 6–25 V, picking up to 5.2 ± 0.1 at 42–60 V, in sample 2 the approximately linear range is limited to 6–8 V, corresponding to field strengths of less than 0.5 V/μm. This might be related to the fact that we use larger gaps (10–20 μm, the BATOP antenna has a 16 μm gap) than typically used for cw THz generation. Simulation data for a gap width of 10 μm (Fig. 6 of Ref. 40) show a remarkably similar shape (straight line in log-log plot, followed by saturation and then picking up again) of the THz-active current versus the applied electric field, which the authors relate to an increase of electron lifetime with bias. However, the scaling exponent for the current is 1.3, giving an expectation of 2.6 and not nearly 4 for the THz-power-voltage characteristic. This is related to the fact that the predicted DC photocurrent increases linearly with voltage in that range, whereas we observe a quadratic behavior as indicated.

As a final observation we note that the characteristic of the DC current versus voltage is not saturating but shows a strong increase (scaling exponent in log-log plot 4.3) in the range where the THz output is saturating (compare Figs. 5(a) and 5(b) in the 60–75 V range). Thereafter, in the 80–90 V range, the exponent drops back to about 2.6 and the THz efficiency increases again. This strong increase of the DC current without a corresponding increase in the THz-active current might be related to the fact that the dark current versus voltage characteristic shows also a strong increase (with a scaling parameter of 5.5 ± 0.2) beyond 55 V, including a small reduction of growth rate beyond 80 V.

IV. SUMMARY AND CONCLUSIONS

The results achieved in this work demonstrate the feasibility of using recessed electrodes for THz generation and indicate great potential for managing the heat dissipation in THz antennas. However, mechanisms of the THz emission at high voltages need to be investigated. It seems beneficial for the efficiency of carrier collection and to benefit from the field enhancement at the electrodes[41] to return to the use of interdigitized fingers within the gap as typically used for cw photomixers.[8,9,41] Interdigitized fingers were not included in the first devices due to the challenges of fabricating recessed structures with typical parameters of a finger width of 0.2 μm and a finger spacing of 1.8 μm.[8,9,41] However, structures on the 1 μm scale have already been demonstrated.[10,35] Due to the improved field distribution,[10,35] recessed electrodes might be the technology of choice even if the diamond is soldered to the back, removing the costs of an optical quality crystal at the expense of a more difficult handling process as indicated previously. An additional benefit of back-mounting is an increased efficiency of THz outcoupling, because the THz radiation goes primarily into the half-plane with the highest dielectric constant and a diamond on the front has a much higher dielectric constant than air and thus reduces the directionality of emission.

The Strathclyde group gratefully acknowledges support from the Research and Development fund of the University of Strathclyde and the Royal Society. S.C. and S.K. were supported by an EPSRC DTA, M. A. by a scholarship of King Saud University. The Manchester group is grateful for STFC for funding some of the THz work described here via the project ST/F003471/1 "High Power Semiconductor Terahertz Frequency Sources For Imaging Applications." We are grateful to J. Roulston, Scimus Solutions Inc., for useful discussions and to Eagleyard Photonics for 850 nm DFB lasers used in first investigations.

[1]M. Tonouchi, Nat. Photonics **1**, 97 (2007).
[2]P. U. Jepsen, D. G. Cooke, and M. Koch, Laser Photonics Rev. **5**, 124 (2011).
[3]E. R. Brown, K. A. McIntosh, K. B. Nichols, and C. L. Dennis, Appl. Phys. Lett. **66**, 285 (1995).
[4]K. A. McIntosh, E. R. Brown, K. B. Nichols, O. B. McMahon, W. F. DiNatale, and T. M. Lyszczarz, Appl. Phys. Lett. **67**, 3844 (1995).
[5]I. S. Gregory, W. R. Tribe, C. Baker, B. E. Cole, M. J. Evans, L. Spencer, M. Pepper, and M. Missous, Appl. Phys. Lett. **86**, 204104 (2005).
[6]S. Preu, G. H. Döhler, S. Malzer, L. J. Wang, and A. C. Gossard, J. Appl. Phys. **109**, 061301 (2011).
[7]I. S. Gregory, C. Baker, W. R. Tribea, M. J. Evans, H. E. Beere, E. H. Linfield, A. G. Davies, and M. Missous, Appl. Phys. Lett. **83**, 4199 (2003).
[8]S. Verghese, K. A. McIntosh, and E. R. Brown, Appl. Phys. Lett. **71**, 2743 (1997).
[9]S. Matsuura and H. Ito, "Generation of cw terahertz radiation with photomixing," in *Terahertz Optoelectronics*, Springer, Topics in Applied Physics, Vol. 97, edited by K. Sakai (Springer, 2005), pp. 157–202.
[10]P. Kordős, M. Marso, and M. Mikulics, Appl. Phys. A **87**, 563 (2007).
[11]H. Ito, F. Nakajima, T. Furuta, and T. Ishibashi, Semicond. Sci. Technol. **20**, S191 (2005).
[12]E. Rouvalis, C. C. Renaud, D. G. Moodie, M. J. Robertson, and A. J. Seeds, Opt. Express **18**, 11105 (2010).
[13]M. I. Amanti, G. Scalari, M. Beck, and J. Faist, Opt. Express **20**, 2772 (2012).
[14]Y. Sasaki, H. Yokoyama, and H. Ito, Electron. Lett. **41**, 712 (2005).
[15]M. Scheller, J. M. Yarborough, J. V. Moloney, M. Fallahi, M. Koch, and S. W. Koch, Opt. Express **18**, 27112 (2010).
[16]J. Kiessling, F. Fuchs, K. Buse, and I. Breunig, Opt. Lett. **36**, 4374 (2011).
[17]M. Scheller, S. W. Koch, and J. V. Moloney, Opt. Lett. **37**, 25 (2012).
[18]A. J. Deninger, T. Göbel, D. Schönherr, T. Kinder, A. Roggenbuck, M. Köberle, F. Lison, T. Müller-Wirts, and P. Meissner, Rev. Sci. Instrum. **79**, 044702 (2008).
[19]D. Stanze, A. J. Deninger, A. Roggenbuck, S. Schindler, M. Schlak, and B. Sartorius, J. Infrared Millim. Terahertz Waves **32**, 225 (2011).
[20]N. Kim, S.-P. Han, H. Ko, Y. Leem, H.-C. Ryu, C. Lee, D. Lee, M. Jeon, S. Noh, and K. H. Park, Opt. Express **19**, 15397 (2011).
[21]D. Saeedkia, R. R. Mansour, and S. Safavi-Naeini, IEEE Trans. Antennas Propag. **53**, 4044 (2005).
[22]A. Dreyhaupt, S. Winnerl, T. Dekorsy, and M. Helm, Appl. Phys. Lett. **86**, 121114 (2005).

[23]G. Matthäus, S. Nolte, R. Hohmuth, M. Voitsch, W. Richter, B. Pradarutti, S. Riehemann, G. Notni, and A. Tünnermann, Appl. Phys. Lett. **93**, 091110 (2008).
[24]A. W. Jackson, "Low-temperature-grown GaAs photomixers designed for increased terahertz output power", Ph.D. dissertation (University of California at Santa Barbara, 1999), cited in Matsuura 2005.
[25]S. Verghese, E. K. Duerr, K. A. McIntosh, S. M. Duffy, S. D. Calawa, C. -Y. E. Tong, R. Kimberk, and R. Blundell, IEEE Microw. Guid. Wave Lett. **9**, 245 (1999).
[26]Z. L. Liau, Appl. Phys. Lett. **77**, 651 (2000).
[27]M. Kuznetsov, F. Hakimi, R. Sprague, and A. Mooradian, IEEE Sel. Top. Quantum Electron. **5**, 561 (1999).
[28]M. Grabherr, M. Miller, R. Jäger, R. Michalzik, U. Martin, H. J. Unold, and K. J. Ebeling, IEEE J. Sel. Top. Quantum Electron. **5**, 495 (1999).
[29]N. S. Daghestani, G. S. Sokolovskii, N. E. Bazieva, A. V. Tolmatchev, and E. U. Rafailov, Semicond. Sci. Technol. **24**, 095025 (2009).
[30]J.-M. Hopkins, S. Smith, C. Jeon, H. Sun, D. Burns, S. Calvez, M. Dawson, T. Jouhti, and M. Pessa, Electron. Lett. **40**, 30 (2004).
[31]R. H. Abram, K. S. Gardner, E. Riis, and A. I. Ferguson, Opt. Exp. **22**, 5434 (2004).
[32]A. J. Kemp, G. J. Valentine, J.-M. Hopkins, J. E. Hastie, S. A. Smith, S. Calvez, M. D. Dawson, and D. Burns, IEEE J. Quantum Electron. **41**, 148 (2005).
[33]A. J. Maclean, R. B. Birch, P. W. Roth, A. J. Kemp, and D. Burns, J. Opt. Soc. Am. B **26**, 2228 (2009).
[34]A. W. Jackson, J. P. Ibbetson, A. C. Gossard, and U. K. Mishrab, Appl. Phys. Lett. **74**, 2325 (1999).
[35]M. Mikulics, S. Wu, M. Marso, R. Adam, A. Förster, A. Hart, P. Kordos, H. Lüth, and R. Sobolewski, IEEE Photon. Tech. Lett. **18**, 820 (2006).
[36]S. Adachi, J. Appl. Phys. **58**, R1 (1985).
[37]T. Rössler, R. A. Indik, G. K. Harkness, and J. V. Moloney, Phys. Rev. A **58**, 3279 (1998).
[38]E. R. Brown, K. A. McIntosh, F. W. Smith, K. B. Nichols, M. J. Manfra, C. L. Dennis, and J. P. Mattia, Appl. Phys. Lett. **64**, 3311 (1994).
[39]BATOP GmbH, "PCA-44-16-16-800-h" (2008); available at http://www.batop.com.
[40]D. Saeedkia, R. R. Mansour, and S. Safavi-Naeini, IEEE J. Quantum Electron. **41**, 1188 (2005).
[41]I. S. Gregory, C. Baker, W. R. Tribe, I. V. Bradley, M. J. Evans, E. H. Linfield, A. G. Davies, and M. Missous, IEEE J. Quantum Electron. **41**, 717 (2005).